

## Min Zhang

Mem. ASME

Laser Processing Research Center,  
School of Mechanical and Electrical Engineering,  
Soochow University,  
Suzhou 215021, Jiangsu, China  
e-mail: mzhang@aliyun.com

## Y. Lawrence Yao

Fellow ASME

Advanced Manufacturing Laboratory,  
Department of Mechanical Engineering,  
Columbia University,  
New York, NY 10027  
e-mail: yly1@columbia.edu

## Chang Jun Chen<sup>1</sup>

Mem. ASME

Laser Processing Research Center,  
School of Mechanical and Electrical Engineering,  
Soochow University,  
Suzhou 215021, Jiangsu, China  
e-mail: chjchen2001@aliyun.com

## Panjawat Kongsuwan

Mem. ASME

Advanced Manufacturing Laboratory,  
Department of Mechanical Engineering,  
Columbia University,  
New York, NY 10027  
e-mail: panjawat.kon@mtc.or.th

## Grant Brandal

Mem. ASME

Advanced Manufacturing Laboratory,  
Department of Mechanical Engineering,  
Columbia University,  
New York, NY 10027  
e-mail: gbb2114@columbia.edu

## Dakai Bian

Mem. ASME

Advanced Manufacturing Laboratory,  
Department of Mechanical Engineering,  
Columbia University,  
New York, NY 10027  
e-mail: db2875@columbia.edu

# Effects of Laser Radiation on the Wetting and Diffusion Characteristics of Kovar Alloy on Borosilicate Glass

*The purpose of this study was to investigate the advantages of laser surface melting for improving wetting over the traditional approach. For comparison, kovar alloy was pre-oxidized in atmosphere at 700 °C for 10 min, and then wetted with borosilicate glass powder at 1100 °C with different holding time in atmosphere. The proposed approach used a Nd:YAG laser to melt the surface of the kovar alloy sample in atmosphere, then wetted with borosilicate glass powder at 1100 °C with the same holding time. The laser melted surface shows a decrease in contact angle (CA) from 47.5 deg to 38 deg after 100 min. X-ray photoelectron spectroscopy (XPS) analysis shows that the surface and adjacent depth have higher concentration of FeO for laser treated kovar (Kovar(L)) than that on traditional thermal treated kovar (kovar(P)). This is attributed to the following improved wetting and diffusion process. The adhesive oxide layer formed on kovar (L) may enhance the oxygen diffusion into the substrate and iron diffusion outward to form an outside layer. This is another way to enhance the wetting and diffusion process when compared to the delaminated oxide scales formed on kovar (P) surface. The diffusion mechanisms were discussed for both approaches. Scanning electron microscope (SEM) revealed that an iron oxide interlayer in the joint existed under both conditions. Fayalite nucleated on the iron oxide layer alloy and grew into the glass. In both cases, neither Co nor Ni were involved in the chemical bonding during wetting process. The work has shown that laser surface melting can be used to alter the wetting and diffusion characteristics of kovar alloy onto borosilicate glass. [DOI: 10.1115/1.4037426]*

*Keywords:* Kovar alloy, borosilicate glass, preoxidation, wetting

## 1 Introduction

The joining of glass to metal has been widely used after the invention of the electric light bulb in the beginning of the nineteenth century. For this invention, a glass bulb was joined to a metal to create an electric contact [1]. Nowadays, such joining is applied in the electronics, medical device and military industry. For most applications, the joints are successful and relatively easy to make. In other applications such as in the nuclear, aerospace, and electronic industry, which requires a long life, temperature stability and hermeticity of glass-to-metal joints is essential. There

have already been many investigations to overcome these difficulties for making high-quality joints between glass and metal, because of the increasing need for such joints.

Because its excellent thermal expansion match to that of borosilicate glass, kovar or Fe–Ni–Co alloy has been widely used to join with borosilicate glass. To achieve a high joint strength and hermetic sealing [2–3], chemical bonding is necessary. For a chemical bond, there must be a continuity of the atomic structure across the interface. This can be obtained by the oxide of the metal that shares the oxygen ions between the glass and the metal. Zhang and Gary [4] pointed that the oxide scale on the alloy dissolves into the glass promoting wetting and bonding at the interface during the glass-to-metal joining.

As reported in literature, the preoxidized layer consisted of hematite (Fe<sub>2</sub>O<sub>3</sub>), wustite (FeO), magnetite (Fe<sub>3</sub>O<sub>4</sub>), and a

<sup>1</sup>Corresponding author.

Manuscript received March 5, 2017; final manuscript received June 21, 2017; published online November 17, 2017. Assoc. Editor: Hongqiang Chen.

complex zone including magnetite and an alloy enriched in nickel and cobalt [5]. It is well understood that sealing with high bonding strength requires three factors: sufficient thickness of the oxide scale on the preoxidized alloy surface; optimum sealing time and temperature for the glass to wet the preoxidized alloy and dissolution of the oxide scale into the glass without devitrification to develop matching dilatometric behavior of the interfacial constituents [6].

However, the interfacial phenomena are not fully understood in this system. For example, it is not clear whether Co or Ni in the alloy plays any significant role in the chemical bonding [7] or whether wustite (FeO) exists as an interlayer in the joint to bridge the metallic bond in the alloy and the ionic/covalent bond in the glass [8]. FeO is the most beneficial substances to enhance the wetting and diffusion ability between glass-to-alloy. Fe<sub>3</sub>O<sub>4</sub> is the second, while Fe<sub>2</sub>O<sub>3</sub> has a negative effect on wetting and diffusion process.

Thus, the oxide scale on the metal surface is very important for glass-to-metal seal (GTMS). Quality of the final joint and whether or not it is hermetic depends on the thickness and type of the oxide scales. Many researchers studied the mechanisms of adhesion between the glass-to-metal sealing [6], but no work has been focused on direct wetting and diffusion of borosilicate glass to laser-surface-melted kovar (Fe–Ni–Co) alloy. As far as the authors know, the bonding system between the laser-surface-melted kovar alloy and borosilicate glass has not been reported. When melted in atmosphere, iron oxides can be formed on kovar alloy and act as interlayer during the following wetting process. The present study aims to clarify these issues, leading to a better understanding of the wetting and diffusion mechanisms for kovar alloy and borosilicate glass.

## 2 Literature Review

Glass-to-alloy binding involves wetting of glass on the alloy surface and subsequent chemical reactions and mechanical bonding [9–12]. Pre-oxidation of alloy is often used to produce a thin and adherent oxide layer on the surface of the alloy. This is generally done by heat treatment at different temperatures and isothermal holding periods depending upon the alloys. Previous studies have reported that the optimum thickness of this layer for achieving high-quality bond is 2–10 μm [13]. Wetting at the interface indicates adhesion of glass to the alloy surface, which will facilitate sealing and joining. Different theories have been proposed for bonding of alloy and glass [14]. Among them, chemical bonding of glass to metal is gradually formed into a transition zone in which the metal-oxide ion on the metal surface is slowly replaced by the ionic-covalent bonding of the glass.

Characteristically, in glass-to-alloy applications, the glass does not bond directly to the alloy, but to an oxide film which is conventionally formed by a thermal treatment on the alloy prior to wetting/bonding. The resulting oxide acts as a transition interlayer in that it is bonded to the underlying alloy and the glass materials. Therefore, the properties of the metal oxide affect the overall properties of the glass-to-alloy bond [15,16]. Improving the oxide scale property which in turn may enhance the wetting behavior between the kovar to glass is a solution to enhance the wettability between glass to alloy. But few papers studied this topic and gave a description of the interaction mechanism [8].

Luo and Shen [17] thought the wetting processing can be divided into three stages: incubation period, reaction period, and equilibrium period. Wang et al. [6] studied the microstructure and strength of borosilicate glass-to-kovar joints. They both used the traditional pre-oxidation methods. Other authors studied the influence of treatment duration and temperature on the oxide scale [6] and focused on the furnace point, hydrogen concentration, and gas type pretreatment to achieve different properties of oxide scales [6,17].

Also, the surface microstructure, such as, grain size, and surface conditions have a great influence on the surface oxidation of

alloys [18–22]. Trindade et al. [18] studied the oxidation behavior of an austenite steel TP347 with different grain sizes. They found that protective Cr<sub>2</sub>O<sub>3</sub> formation is promoted by a high density of fast grain-boundary diffusion paths which is the case for fine-grained materials. Geng et al. [19] once fabricated nanocrystalline coating of a low-Cr Fe–Co–Ni base alloy with 0.36 wt % Si was deposited on the as-cast low-Cr alloy with identical compositions by means of magnetron sputtering. It was found that the columnar nanograin structure significantly lowered the oxidation rate and changed the surface oxide structure of this alloy. The formation of a continuous Cr<sub>2</sub>O<sub>3</sub> inner layer beneath the CoFe<sub>2</sub>O<sub>4</sub> spinel outer layer on the sputtered nanocrystalline coating resulted in a remarkable improvement in oxidation resistance compared to the cast low-Cr alloy. Zhang et al. [20] once reported that the nanocrystalline alloys were prepared by direct current magnetron sputtering coating. Weight change kinetics were measured by continuous thermogravimetry. For microcrystalline alloy in dry air, a small initial weight gain was followed by gradually increasing spallation [20]. Nanocrystalline 304SS, underwent relatively rapid oxidation in the very early cycles of reaction, but then the reaction slowed down [20]. No spallation was apparent in either gas. The weight gain was higher in wet air than in dry air. In both gases, a dense and continuous chromium oxide layer was formed at the surface, together with other oxides distributed inside the coating layer [20]. The result of Liu et al. [21] demonstrated that contribution of grain refinement to the oxidation is predominantly due to its effect on the inward oxidation process. Decreasing grain size promoted intergranular oxidation, accelerated formation of the Cr-containing inner scale, contributed to the faster transition to the steady-state oxidation and correspondingly slightly improved the oxidation resistance [21].

During wetting/bonding process, the interfacial phenomena of wetting are often the primary factor governing whether a coating will bond to a substrate in practical applications such as glass-to-alloy wetting. To date, very few publications are concerned with the use of lasers to enhance wettability characteristics. Previously, the use of laser surface texturing for wettability control has been reported on polymeric [22,23] and metallic materials [24–27]. This phenomenon is the consequence of the air entrapment as explained in Cassie–Baxter model [26]. It has been shown that the hierarchical surface textures composed of micro- and nanofeatures on metallic surfaces were initially hydrophilic (contact angle (CA) = 20 deg) and in time became hydrophobic (CA = 150 deg) [25].

As to use laser melting to enhance the wettability of steel, there is few literature reported. Kam et al. [27] found that during surface wettability experiments, the contact angle of water varied from 0 deg (superhydrophilic) to 113 deg on laser microcone textured surfaces depending on processing conditions. Additionally, a superhydrophobic AISI 316L stainless steel surface was created (contact angle ~150 deg) with a functionalized silane coating on already hydrophobic surface geometry. Lawrence and Li [28] concluded that high-power diode laser radiation can be used to alter the wetting characteristics of carbon steel so as to facilitate improved enameling.

It is observed that the common practice in oxidation of kovar alloy involves the use of furnace thermal treatments. These processes are prone to environmental changes and are nondeterministic in nature. The oxide scales are expected to form on the entire alloy surface, which can be unacceptable under circumstances where only the contacted area should be oxidized. Moreover, oxidizing the entire alloy surface could be harmful to its mechanical and physical properties. Laser surface melting can be used to control surface micro- and nanotopography to reduce contact angle, as well as provide increased area and anchoring points to increase resistance to adhesion failure. Iron has a high affinity to oxygen and especially at elevated temperatures reacts to form FeO, Fe<sub>2</sub>O<sub>3</sub>, or Fe<sub>3</sub>O<sub>4</sub>. Such affinity is expected to cause an oxide scale formed on the melted surface, reducing the apparent contact angle. The use of laser surface melting allows selective and

repeatable processing conditions, which can be adapted to local or large area treatments.

In this work, the use of a Nd:YAG laser source to alter surface structure of kovar alloy is studied to control wetting behavior with the aim of improving adhesion. A single-step strategy based on surface remelting is employed to substitute the commonly used thermal oxidation in furnace. These treated surfaces are extensively studied in terms of surface chemistry and microstructure. The enhanced wettability is expected through this method.

### 3 Experimental

**3.1 Materials Preparation.** The chemical composition of the Kovar alloy (ASTM F15) used in the present work is supplied by Edfagan company. The chemical composition is 28.85%Ni, 53.47%Fe, 17.15%Co, 0.17%Mn, 0.15% Si, 0.03% Ti, 0.03% Cu, 0.012%Al and minor amounts of Mo, Zr, and C (in wt %). The kovar alloy was cut into pieces of 25 mm × 15 mm × 1 mm and ultrasonically cleaned with acetone.

The borosilicate glass powder (Mountain Glass Company, Asheville, NC) used in present study had a composition of 3.7 NaO<sub>2</sub>, 3.8 K<sub>2</sub>O, 30.0 Al<sub>2</sub>O<sub>3</sub>, 23.0 B<sub>2</sub>O<sub>3</sub>, and SiO<sub>2</sub> is the balance (in weight percentage). For the wetting experiment, the glass ingot was 200 mg with a diameter of 2.5 mm and thickness of 3 mm.

Laser surface melting was carried out using a GSI Lumanics JK-2000 laser, operating at 400 W, with a 1 mm beam diameter and a traverse speed set at 6 mm/s. It was melted under atmosphere without protecting gas, allowing the oxygen in the atmosphere to react with the alloy. A multiple pass laser surface treatment, with an overlap between successive laser melted tracks of approximately 20%, was applied to the kovar samples.

**3.2 Wetting Procedure.** The Sessile drop technique was used in the wetting process. The glass ingot was prepared and placed in the center of the kovar alloy sample. Preoxidized kovar alloy samples were used for experiments. The samples were heated under 1100 °C at the ramping-up rate of 3 °C/min in a tube furnace for a holding time of 30 min, 100 min, 160 min, 240 min, and 300 min, respectively. Glass ingot dimension is  $\Phi 2.5 \times 3$  mm, and each glass ingot has a weight of 200 mg. The samples were prepared by standard metallographic procedures to measure the wetting angle using an optical microscope (OLYMPUS, BX60, Japan).

**3.3 Microscopic Observation and Elemental Analysis.** The samples are trimmed and polished using the routine metallurgical method and etched with 10% Nital (10% nitric acid+90% alcohol). Then, the oxidation scale formed after the high temperature oxidation treatment and the glass-to-metal interface is observed using the optical microscope. The samples were characterized by scanning electron microscopy (SEM, S-4700 model) after polishing. Energy dispersive X-ray spectroscopy (EDX) analysis was carried out in order to detect any elemental diffusion into or away from the bonding and to examine any chemical interactions between the glass-to-kovar interface. Rectangular pieces of kovar alloy with dimension of 8 mm × 8 mm × 1 mm were cut for X-ray photoelectron spectroscopy (XPS) analysis. Both the surface and the depth XPS spectra were collected and compared with the preoxidized and laser melted kovar Fe–Ni–Co alloy. For depth profiling, Ar<sup>+</sup> ions were used to sputter 20 s and 40 s, respectively.

## 4 Results and Discussion

**4.1 Characterization of Pre-Oxidated and Laser-Treated Samples.** Figure 1 presents typical optical (Fig. 1(a)), and SEM (Fig. 1(b)) cross section micrographs of a laser-treated kovar specimen. Three different zones can be identified in the microstructure. The surface region is the laser melted and resolidified zone

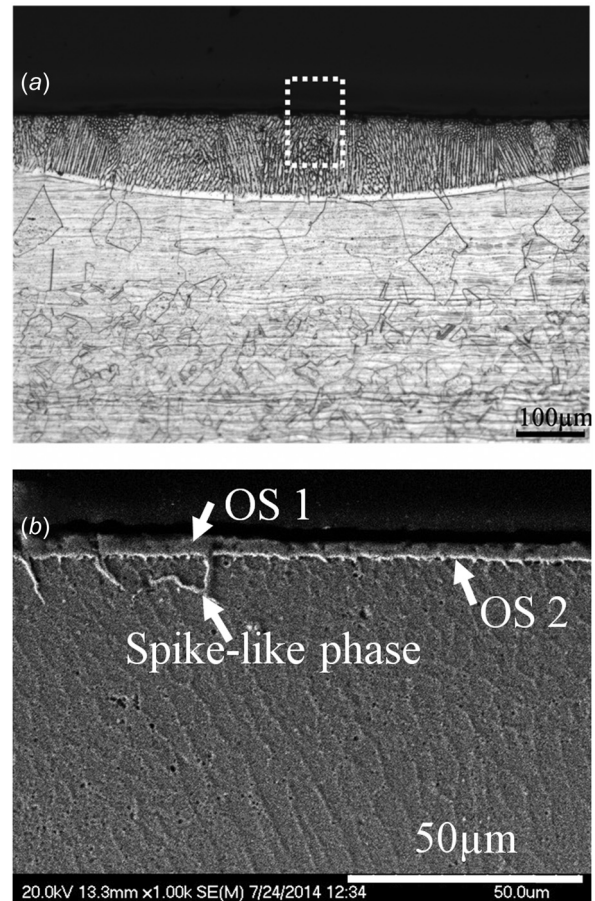


**Fig. 1 Microstructure of the cross section for laser melted zone: (a) optical microscopy and (b) high magnification of the white framed area shown in Fig. 1(a) (OS 1-oxide scale 1, OS 2-oxide scale 2)**

with depth of 65–115  $\mu\text{m}$ . Below it there is a zone of approximately 7–14  $\mu\text{m}$  in depth, which is the heat affected zone where some modified and unmodified regions coexist and below it the as-received alloy remains unaltered. The grain size in the melted zone ranges from 7  $\mu\text{m}$  to 23  $\mu\text{m}$ , while the untreated kovar substrate has grain size ranging from 23 to 94  $\mu\text{m}$ . There is columnar-cell crystalline structure in the refined grain size zone. The refined grain size may affect the oxidation process in the wetting process. There exists a thin oxide layer on the surface, and it is revealed by the high resolution of SEM shown in Fig. 1(b). The surface oxides scale can be divided into two layers, oxide scale 1 has a thickness approximately 3.8  $\mu\text{m}$ , while oxide scale 2 about 1.1  $\mu\text{m}$ . In addition, no spallation of oxide scale can be found at the oxide scale/kovar interface. A spike-like phase has a depth of about 11.1  $\mu\text{m}$ . It is formed due to oxygen transfer through the grain boundary into the substrate.

Figure 2 shows the cross section view of the kovar sample oxidized at 700 °C with a holding time of 10 min. The oxide layer has about 5.2  $\mu\text{m}$  in thickness as shown in Fig. 2. Loughridge and Wong [29] suggested that a kovar oxide layer between 2  $\mu\text{m}$  and 10  $\mu\text{m}$  in thickness promoted strong bonding in production of matched glass-to-metal seals, which is in agreement with the present observation. Contrasting to the oxide scales grown tightly together as shown in Fig. 1, there is a visible gap between the oxide scale 1 and oxide scale 2 in this thermal treatment. The oxide scale 1 has a thickness of 2.4  $\mu\text{m}$  and oxide scale 2 has a thickness of about 2.9  $\mu\text{m}$ . The spike-like phase has a length of about 6  $\mu\text{m}$ . When compared to Fig. 1, tight oxide scales formed on the laser treated sample, while spallated oxide scales formed

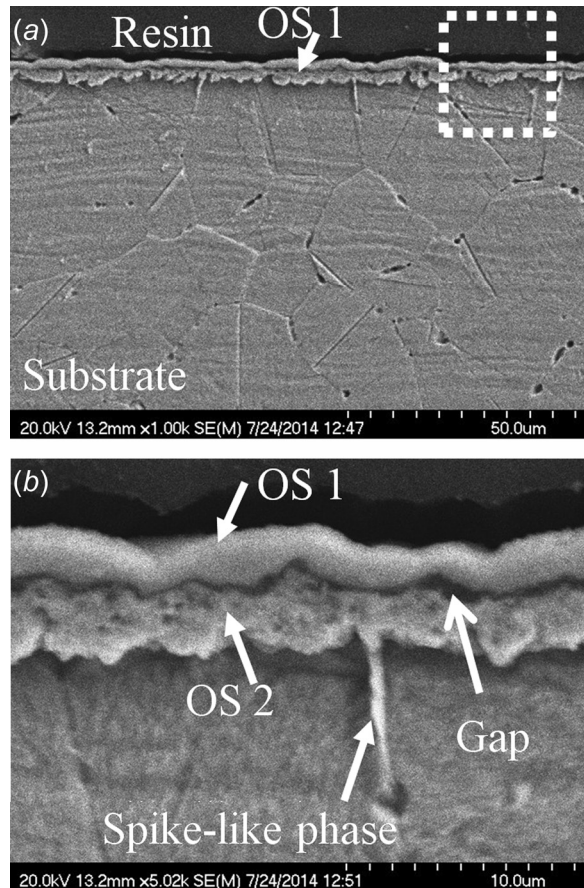


**Fig. 2** (a) Cross section of pre-oxidized Kovar alloy showing oxide and substrate under 700 °C and holding time of 10 min in atmosphere and (b) the high magnification of the framed area shown in (a) (OS 1-oxide scale 1, OS 2-oxide scale 2)

on preoxidized sample. The tight oxide scales formed on the kovar surface may improve the quality of interface between glass and metal. Also, the spikelike phase formed by laser process has a longer distance compared to the pre-oxidation sample, which in turn indicates that the oxygen has a higher diffusion ability. Considering the presence of the spikelike phase, the practical contact areas of oxides and kovar substrate will increase due to the so-called pegging effect, which would improve the bonding strength between oxides and kovar substrate. The tight oxide scales and the longer distance of spikelike phase may be beneficial to the subsequent wetting and diffusion process in glass to kovar joining. According to the results reported in Ref. [21], the two oxide scales should contain different iron oxides.

The chemical state of the iron oxides surface was investigated with XPS analysis. Figure 3 shows the XPS of Fe 2p spectra of the kovar alloy after laser (abbreviated as kovar (L)) and pre-oxidized treat (abbreviated as kovar (P)). The Fe 2p XPS spectra have long been known to be complex because of the large amount of coupling between the core hole states produced by photoemission process and the high spin states of iron [30,31]. The percentage of each oxidation state of Fe was deduced by peak fitting using Shirley background subtraction method. As shown in Fig. 3, however, the 2p peaks of iron oxides cannot be fitted with a single symmetric Gaussian/Lorentzian peak because strong multiplet splitting results in an asymmetric peak shape. Taking into account the results shown in Figs. 1 and 2 together with results in Refs. [21,30], and [31] and the spectral features, the surface spectrum of the samples can correspond to pure Fe<sup>2+</sup> and Fe<sup>3+</sup>. From Fig. 3(a), it can be clearly observed that the Fe 2p<sub>1/2</sub> and 2p<sub>3/2</sub> peaks located at around 710.9 and 724.7 eV are broadened due to

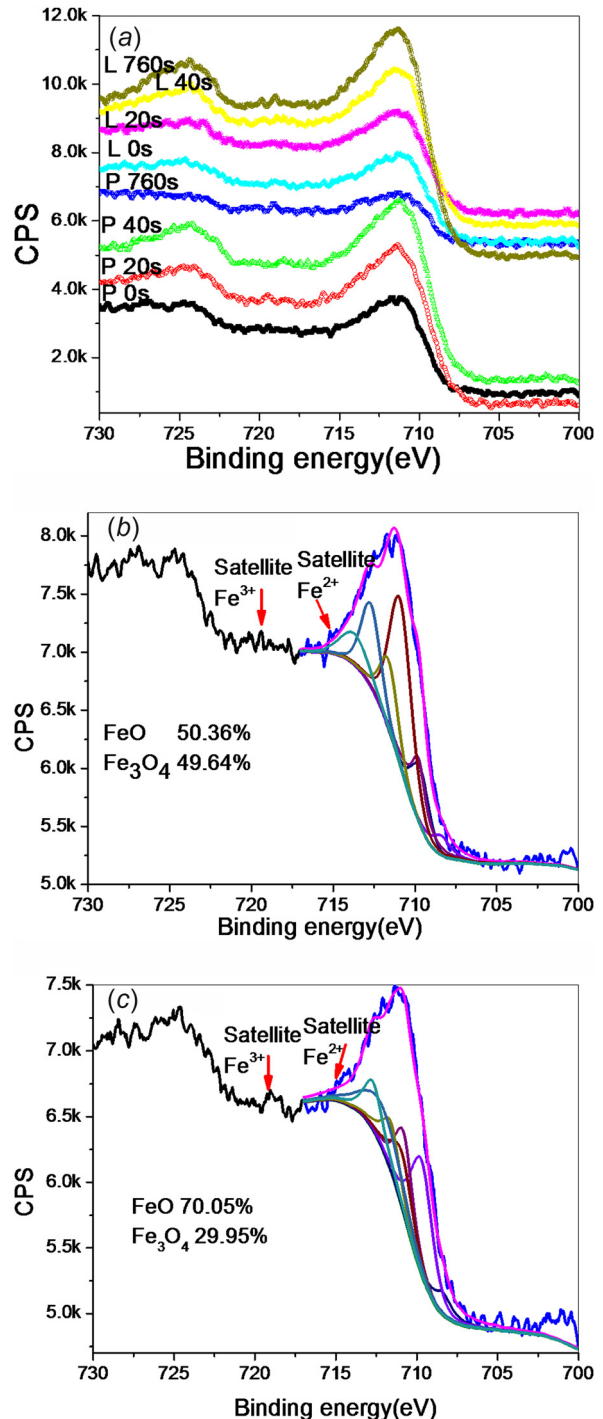


**Fig. 3** Fe 2p XPS spectra of (a) as received, (b) pre-oxidized, and (c) laser treated Kovar sample surface

the existence of both Fe<sup>2+</sup> and Fe<sup>3+</sup> ions with Fe<sub>3</sub>O<sub>4</sub> being the mixed state of FeO and Fe<sub>2</sub>O<sub>3</sub> [30,31]. The present values match very well the previously reported ones [30,31]. Due to the fact that the binding energy levels of the satellite peaks of Fe 2p<sub>3/2</sub> for different Fe oxidation states Fe<sup>2+</sup> or Fe<sup>3+</sup> occur at 715 or 719 eV, respectively, the satellite peaks can be used to identify the presence of FeO, Fe<sub>2</sub>O<sub>3</sub> or Fe<sub>3</sub>O<sub>4</sub>. The small peaks (satellite peaks) occur at around 719 eV can be used to reveal the presence of Fe<sub>2</sub>O<sub>3</sub>. And the small peak exists at around 715 eV can be used to prove the presence of FeO. The small peaks (satellite peaks) exist at around 715 eV and 719 eV can reveal the formation of Fe<sub>3</sub>O<sub>4</sub> in the present study. Due to Fe<sub>3</sub>O<sub>4</sub> consists of FeO·Fe<sub>2</sub>O<sub>3</sub>, so the

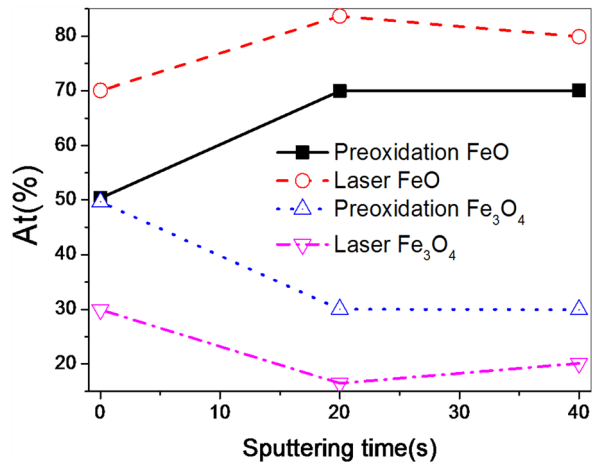
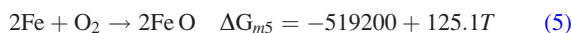
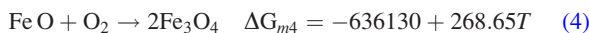
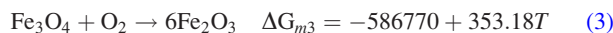


Fig. 4 XPS depth profiles for laser treated and pre-oxidation Kovar samples

Fe<sub>3</sub>O<sub>4</sub> can be expressed as Fe<sup>2+</sup>.2Fe<sup>3+</sup>. Through this method, we can calculate the concentration of different iron oxides. Figures 3(b) and 3(c) demonstrate the surface composition for kovar (P) and kovar (L). They both show FeO and Fe<sub>3</sub>O<sub>4</sub> iron oxides but with different concentrations.

Figure 4 illustrates the XPS depth profile with FeO and Fe<sub>3</sub>O<sub>4</sub> concentrations estimated by the calculation procedure described in the paragraph above. The FeO content increases from 50.36% to 70.07%, and 70.05% to 79.87% for Kovar (P) and Kovar (L), respectively. While the relative Fe<sub>3</sub>O<sub>4</sub> concentration drops from initial 49.64–29.93%, and 29.95–20.13% for Kovar (P) and Kovar (L), respectively. The higher concentration of FeO in the surface and the region immediately below it is beneficial to the chemical bonding of glass-to-metal sealing. There has a higher concentration of FeO concentration in Kovar (L) when compared to Kovar(P), which in turn can contribute positively in the subsequent wetting and diffusion process.

The free energy of forming metal oxides of the main elements of Fe, Ni, and Co in Kovar alloy when heated in 700 °C and 1450 °C can be calculated following Ref. [32]. As Kovar melting point is 1450 °C, we assume the surface temperature is 1450 °C for the following discussion. For pure iron, there are three different oxides, i.e., wustite (FeO), magnetite (Fe<sub>3</sub>O<sub>4</sub>), and hematite (Fe<sub>2</sub>O<sub>3</sub>). Among the Fe, Ni, and Co elements in Kovar alloy, Fe requires the lowest free energy for oxidation, and thus Fe is the first element to be oxidized at 700 °C and 1450 °C. According to Ref. [32], for Kovar (P), FeO forms first and quickly on the Kovar alloy surface. According to Eqs. (1)–(5)



due to Fe<sub>2</sub>O<sub>3</sub> has a higher oxygen concentration and FeO has the lowest oxygen concentration, the oxide scale formed on Kovar surface from the innermost to the outmost should be Fe/FeO/Fe<sub>3</sub>O<sub>4</sub>/Fe<sub>2</sub>O<sub>3</sub> in theory. The thickness ratios of oxide scales vary with the holding temperature, growth process, and oxygen content. In the present study, from Eqs. (1)–(5), Fe<sub>2</sub>O<sub>3</sub> formation should be through the formation of FeO first, which reacts with oxygen and turns into Fe<sub>3</sub>O<sub>4</sub>, Fe<sub>3</sub>O<sub>4</sub> further reacts with oxygen to form Fe<sub>2</sub>O<sub>3</sub>. The conversion of oxygen to oxygen ion is the

slowest step and this process becomes a rate determining step during the whole process. The oxidation of Fe includes the diffusion of Fe<sup>2+</sup>, Fe<sup>3+</sup>, and oxygen ions (O<sup>2-</sup>). Oxygen ions are difficult to diffuse through the compact oxides scale (Figs. 1 and 2). This diffusion is more difficult for Kovar (P) because there exists a gap between the two oxide scales (Fig. 2(b)). At the initial oxidation stage, since the mole of Fe<sub>3</sub>O<sub>4</sub> forming on the FeO is much smaller than that of FeO, Fe<sub>3</sub>O<sub>4</sub> is dispersed on the FeO surface. The surface oxygen has much higher partial pressure than that below the FeO layer. O<sup>2-</sup> quickly diffuses to the FeO/Kovar interface, and internal oxidation (spikelike phase shown in Figs. 1(b) and 2(b)) is developed at the grain boundaries of the Kovar alloy substrate near the oxide scale/Kovar interface due to internal oxidation. So under both situations, i.e., Kovar(P) and Kovar(L), the outermost layer contains mainly Fe<sub>3</sub>O<sub>4</sub> and FeO.

David [33] proposed that the Fe ions would diffuse outwards through Fe<sub>3</sub>O<sub>4</sub>, but only Fe<sup>3+</sup> would diffuse outward through Fe<sub>2</sub>O<sub>3</sub>, resulting in outward growth of these oxides, Magnetite(Fe<sub>3</sub>O<sub>4</sub>) may form at the magnetite–hematite interface by the following reaction: Fe<sup>n+</sup> + ne<sup>-</sup> + 4Fe<sub>2</sub>O<sub>3</sub> = 3Fe<sub>3</sub>O<sub>4</sub>. New hematite may form at the hematite–gas interface according to the reaction: 2Fe<sup>3+</sup> + 6e<sup>-</sup> + (3/2)O<sub>2</sub> = Fe<sub>2</sub>O<sub>3</sub>. Because during the pre-oxidation process or laser melted process, there exists enough oxygen in the atmosphere and thus on Kovar (P) and Kovar (L) alloy surface, the reaction indicated in Eq. (5) occurs easily and first. As a result, the surface can form FeO and Fe<sub>3</sub>O<sub>4</sub> and is very difficult to form Fe<sub>2</sub>O<sub>3</sub> and thus the final oxide scale mainly contains FeO and Fe<sub>3</sub>O<sub>4</sub>. For the laser treatment, FeO forms quickly and FeO reacts with oxygen to transform into Fe<sub>3</sub>O<sub>4</sub>. But there is not enough time for Fe<sup>3+</sup> in Fe<sub>3</sub>O<sub>4</sub> to change into Fe<sub>2</sub>O<sub>3</sub>. So the laser treated surface also mainly contains Fe<sub>3</sub>O<sub>4</sub> and FeO.

**4.2 Wettability and Diffusion Characteristics.** Figure 5 shows the top view of glass on Kovar (P) wetting for 100 min and the glass already began to soften and be wetted to the Kovar. Also, a halo was found at the fringe between glass and Kovar as indicated by number 1 in Fig. 5. A similar phenomenon was reported by Luo and Shen [17]. This halo represents an interaction region between glass and oxide scale during the wetting process.

Figure 6 shows the contact angle as a function of holding time for wetting of Kovar alloy with borosilicate glass in atmosphere at 1100 °C. Kovar (P) samples heated in furnace at the same temperature and the same holding time showed poorer wettability than those that was treated by laser surface melting. The initial contact angles with a holding time of 100 min, 38 deg and 47.5 deg for Kovar (L) and Kovar (P), respectively. Lawrence and Li [34] pointed that Nd:YAG treatment can lead to a considerable decrease in contact angle due to the increase in the polar component of the surface energy. Such an increase in the polar component of the surface energy of the Kovar alloy has a positive effect on the action of wetting and adhesion [33].

To determine the wettability and diffusion phenomenon for glass-to-Kovar alloy, Fig. 7 shows SEM cross section micrographs of the reaction layer at the halo region with a holding time of 100 min. The reaction layer between resin and porous Fe-depleted zone (I) (which is confirmed in Fig. 8) has a thickness of 147–277 μm (for glass to Kovar (P)) and 232–315 μm (for glass to Kovar (L)), respectively. Examination of Kovar (P) to glass (Fig. 7(a)) shows some porosity but the pores are closed, indicating that this glass-to-kovar (P) sealant will provide high gas tightness and a hermetic structure. A good adhesion between glass-to-alloy can be observed for both cases. While for Kovar (L) to alloy sealant (Fig. 7(b)), there are no visible pores or cracks, which can provide not only gas tightness and a hermetic structure, but also provide good mechanical properties in actual applications.

To clearly depict the different zones from glass to alloy structures, five distinct domains are identified: (a) the original Kovar alloy (not shown in Fig. 7); (b) the zone I indicates porous Kovar

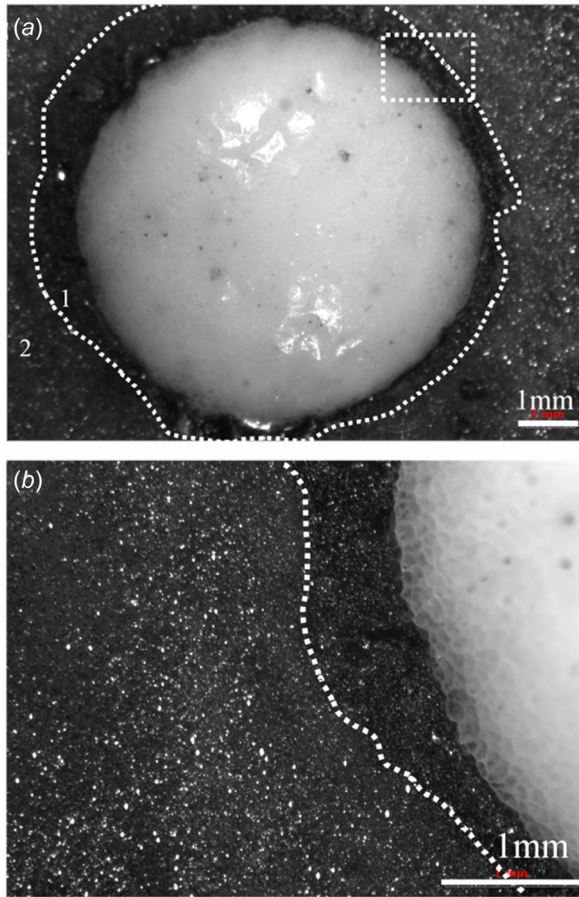


**Fig. 5** Typical appearance of postwetting showing glass spreading on kovar alloy (100 min for pre-oxidized kovar): (a) low magnification and (b) high magnification of the framed area shown in Fig. 5(a)

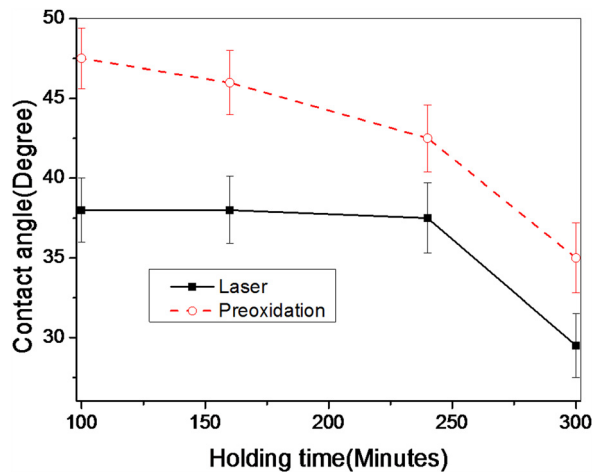


**Fig. 6** CA as a function of time for wetting of kovar by glass at 1100°C with different holding time for pre-oxidized and laser treated sample (The error bar is based on standard deviation)

zone (as confirmed as Fe-depleted zone in Figs. 10 and 11). It is also known as the internal oxidation zone. In this zone, internal oxide scale thickness for Kovar (L) is about 121.95  $\mu\text{m}$ , longer than that in Kovar (P) which is only 109.76  $\mu\text{m}$ ; (c) the reaction layer (as confirmed as FeO interlayer in Figs. 10 and 11). This reaction layer will act as the transition layer between substrate

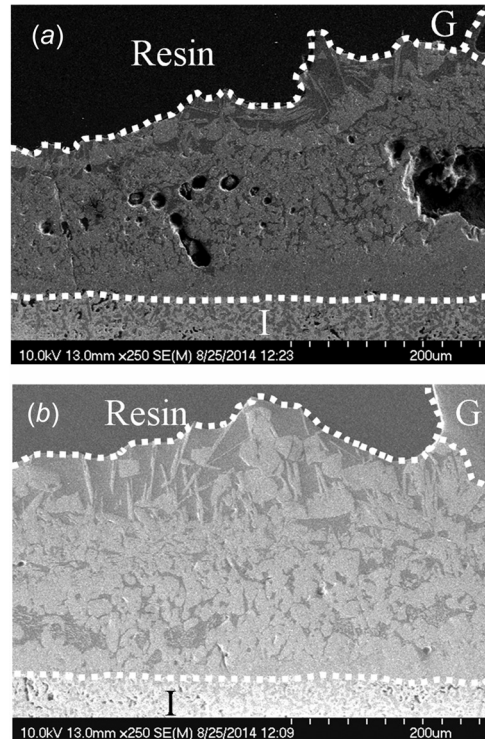


**Fig. 7** Microstructure of the different zone after wetting for (a) kovar (P) and (b) kovar(L), (1100°C with holding time of 100 min; I indicates porous kovar internal oxidation; G indicates glass zone)

alloy and glass. The thickness in Kovar (L) is larger than that in Kovar (P); (d) the mixed zone (as confirmed as mixed zone of glass and  $\text{Fe}_2\text{SiO}_4$ ). In this area, the phase distributes more uniform in Kovar (L) than that in Kovar(P); and (e) the glass zone shows the borosilicate glass.

Figures 8(a) and 8(b) show the micrographs of the borosilicate glass to Kovar alloy interface near the central region of the interface. In the Kovar (P) case (Fig. 8(a)), it can be seen that an interfacial layer formed between the glass and the alloy, but interfacial delaminations (gap) can be obviously seen. This interfacial delaminations are formed due to the loosely compacted oxide layer, which is clearly shown in Fig. 2(b). While in the Kovar (L) case (Fig. 8(b)), no such interfacial delaminations occur and the interface between the glass and kovar alloy is continuous and compact. This is due to the compact oxide layer formed during the laser treatment process. In addition, the Fe-depleted interface is thicker than that in Kovar (P) case. Figure 8(c) shows the EDX line scan and elemental distribution at the interface shown in Fig. 8(b). It is evident that in the zone (denoted as I) Fe is significantly reduced due to the oxygen diffuses inward to form the inner oxide scale through the grain boundaries and iron migrates outward to form the out interface layer. In the formed compact oxide scale together with the refined grain size (shown in Fig. 1), there exists extra vacancy sinks which suppress cavity formation at the oxide scale to alloy interface and thus allow initially fast oxygen diffusion inward and iron diffusion outward through the oxide formed on Kovar (L) surface. This compact oxide scale on Kovar (L) can act as either leakage paths for easy diffusion or a steeper cation vacancy gradient, or both [21]. While for Kovar (P), the interfacial delaminations (gaps) and poorer oxide scale to Kovar alloy contact formed in the pre-oxidation process may hinder the continuous oxygen diffusion inward and iron diffusion outward. As a result, the initial diffusion rate is restrained and suppressed [21] and the interface layer is not as thicker as that in Kovar(L).

Figure 9 shows the relationship between thermal treatment holding time and the thickness of internal oxidation scale. The

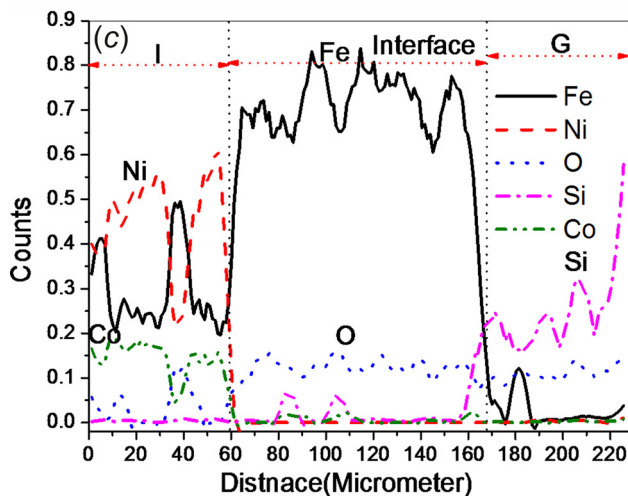
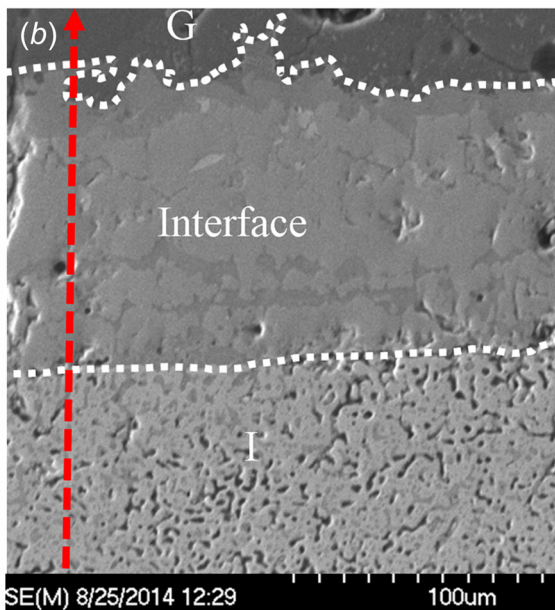
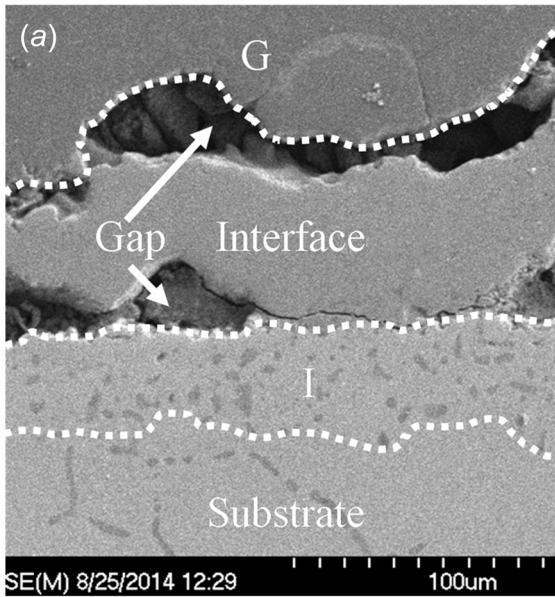


Fig. 8 (a) SEM micrograph of kovar (P) to alloy interface in the central region, (b) SEM micrograph of kovar (L) to alloy interface in the central region, and (c) element line scan along the dotted arrowed line shown in Fig. 8(b)

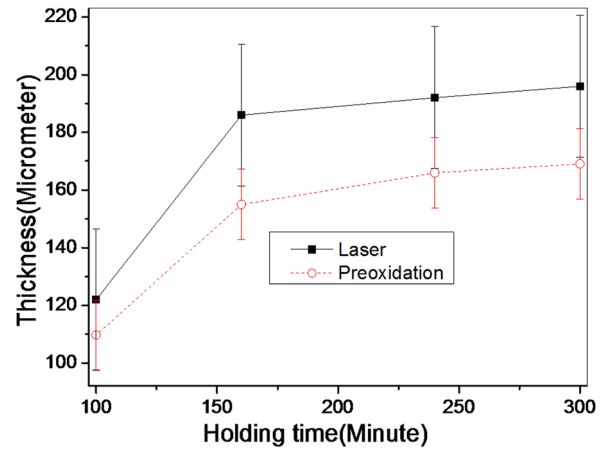


Fig. 9 Relationship between internal oxidation thickness (zone I shown in Fig. 7) for Kovar (P) and kovar (L) with different holding time (The error bar is based on standard deviation)

thickness of the internal oxidation scale for kovar (L) is thicker than that that for kovar (P) due to better diffusion capability. The thickness rises rapidly before it levels off. It indicates that after a long holding the oxygen ions diffusion becomes harder than that in initial time.

Figure 10(a) shows a SEM micrograph of the cross section of the glass/kovar(P) interfacial region wetted at 1000°C for 160 min. The SEM microscope is focused on the central region of the glass/kovar sample. It is evident that no interfacial delamination at the glass/Kovar(P) interfaces took place. The interface between the glass/kovar(P) samples are continuous. Figure 10(b) shows element distribution of Fe, Ni, Co, Si, and O in the interfacial region characterized by EDX line scanning. It can be clearly seen that interdiffusion occurs at the interface, element of Fe diffuses into glass and element of Si in glass diffuses into Kovar. The EDX line scanning results shown in Fig. 10(b) indicates that three regions can be distinguished from left to right in the interfacial region. The content of Fe in region I is varied and the contents of Ni, Fe and O remain almost constant. This zone is considered Fe-deplete and it is formed during oxidation and wetting due to inward oxygen diffusion. The results is consistent with previous works reported by Wang et al. [6]. Due to preferentially oxidized grain boundaries in the bulk, an internal/intergranular oxidation mechanism dominates, by which the scale grows inward (Fig. 3) and thus formed the porous zone. This internal oxidation phenomenon was also reported by Trindade et al. [18]. Region II is the interlayer about 142 µm in thickness. The distinct characteristics of this zone are the absence of Co and Ni, the presence of Fe and O, trace of Si. This zone is referred to as FeO containing Si interlayer. The zone III is the mixed zone contains Fe<sub>2</sub>SiO<sub>4</sub> and undissolved oxides of glass [17]. The far right zone not shown in this figure is the borosilicate glass base.

Figure 11 shows SEM image and EDX line scans of the interface of the glass/kovar (L) samples wetted at 1100°C and holding 160 min in atmosphere. The microstructure can be clearly divided into five zones (including Kovar base and glass dominated zone not shown in the figure). Region I is the porous Fe-depleted zone which is formed due to the scale grows inward and Fe reacts with oxygen. Region II is the interlayer referred to FeO layer, which is mainly composed of Fe and O and some Si diffused from glass. Similar to Fig. 10(b), Ni and Co are not detected in this zone. This FeO containing Si interlayer is about 154 µm and it is thicker than that shown in Fig. 10(b). Region III is the Fe and Si rich zone. This zone is formed due to dissolution of iron oxides and Fe diffusion into the borosilicate glass base. Region III is the mixed zone containing Fe<sub>2</sub>SiO<sub>4</sub> compounds and glass. These results are in agreement with previous studies [4,5,8,15,17] and better than those obtained for the pre-oxidized

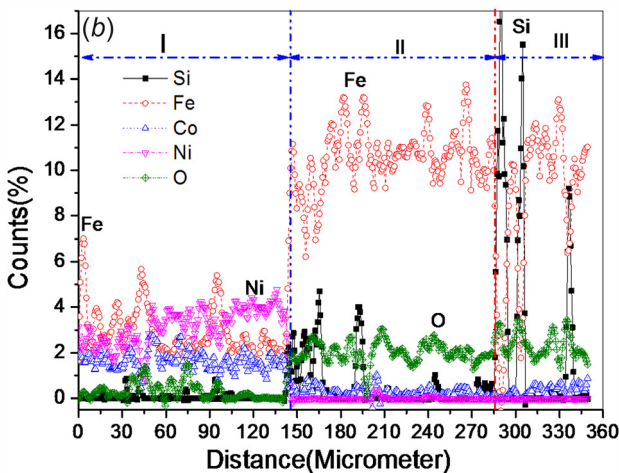
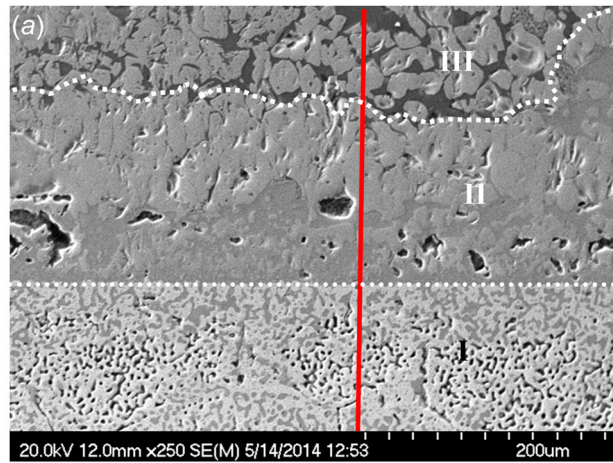


Fig. 10 (a) SEM microscope and (b) EDX line scan along the vertical line shown in Fig. 10(a) for kovar pre-oxidized at 700 °C for 10 min, and then wetted at 1000 °C for 160 min (I indicates porous kovar internal oxidation; II shows interlayer; and III is the mixed zone between glass and  $\text{Fe}_2\text{SiO}_4$  phase)

Kovar. The thicker FeO interlayer in the interface is believed to yield better thermal expansion matching.

**4.3 Bonding Mechanism.** Wustite exist as an interface in the binding of glass-to-alloy to bridge the difference. In present work, a wustite interlayer exists in both Kovar (L) and Kovar (P). The formation of fayalite ( $\text{Fe}_2\text{SiO}_4$ ) is because, after dissolution of the pre-oxidation oxide scale into the molten glass, further oxidation of iron occurred during wetting. The outward diffusion of Fe ions through wustite interlayer extends into the molten glass and formed fayalite ( $\text{Fe}_2\text{SiO}_4$ ). Oxygen diffuses from the molten glass through the wustite interlayer to form the porous Fe-depleted zone.

The fine and homogeneous microstructure is formed in the laser melted layer and the surface contains oxygen. At the initial wetting stage, interface reaction dominates and preferential oxidation occurs at the grain boundaries. More path support as an oxygen to diffuse into the Kovar base due to refined grain size. When the scale reaches a given thickness with the increased wetting time, the process of oxidation in Kovar (L) is restrained and precludes internal oxidation, thus metal ion transport becomes the control step. The  $\text{Fe}^{2+}$  in the melted surface tends to diffuse outward from the substrate to external oxide-glass interface and from the oxides. The outward diffusion of Fe is complemented by solid-state diffusion and diffusion of oxygen from the glass into the Kovar through the oxide scale.

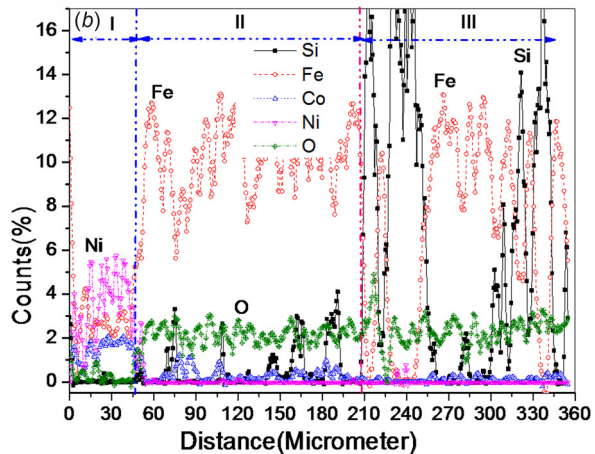
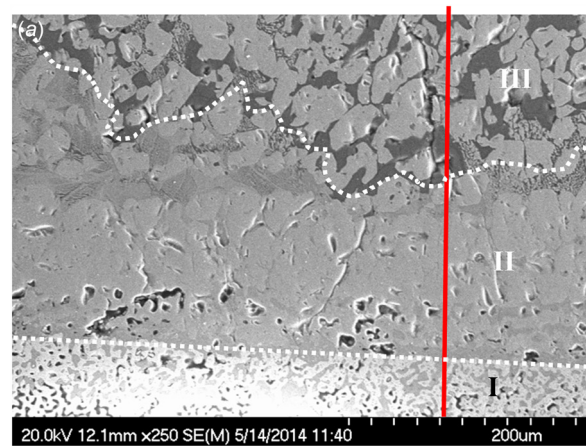


Fig. 11 (a) SEM microscope and (b) EDX line scan along the vertical line shown in Fig. 11(a) for laser treated sample without pre-oxidation, and then wetted at 1000 °C for 160 min

It is well known that the nucleation of the passive film generally occurs at the defects, dislocations, grain boundaries and junctions of the grain boundaries, all of which are known as the active sites. As compared to the coarse-grained structure, the abundant boundaries in the refined size structures can afford more active sites. Some of these active sites would turn into the nucleation sites when their energy exceeds a certain value and the oxide film will form at these sites first. Obviously, more nucleation sites lead to a higher formation rate of the oxide film. The refined grain size in Kovar (L) can afford much more active sites compared with Kovar (P). The most probable active sites for the original sample locate at the junction of the coarse-grain boundaries. The active sites in the refined Kovar are in high-energy state and most of them would turn into the effective nucleation sites. The  $\text{O}^{2-}$  and  $\text{Fe}^{2+}$  will form at these locations first at the initial stage of the wetting, and then spread over the surface until the refined size is completely grown into coarse sizes under high temperature process. More nucleation sites lead a higher formation rate of the  $\text{O}^{2-}$  and  $\text{Fe}^{2+}$  transfer rate and a shorter time required for the entire refined size zone. Therefore, the refined size in Kovar(L) accelerates the  $\text{O}^{2-}$  and  $\text{Fe}^{2+}$  transfer rate during the wetting process, especially in the two-dimensional direction.

When borosilicate glass (the main content is  $\text{SiO}_2$ ) is placed on Kovar alloy which contains a FeO oxide layer, solution of FeO occurs (reacting with  $\text{SiO}_2$  and form  $\text{Fe}_2\text{SiO}_4$ ) resulting in immediate saturation of the liquid at the interface with the oxide. The solution rate of the remaining oxide mainly depends on diffusion into the bulk FeO-unsaturated glass [35]. And the good adherence of glass on alloy can be obtained, resulting from the diffusion and saturation of the glass at the interface with FeO oxide [35]. So the

higher concentration of FeO formed on Kovar (L) can further enhance the wetting and diffusion process.

## 5 Conclusion

The laser surface melting results in rapid heating of the surface and consequently leads to the refined grain size and more grain boundaries, which serve as paths for oxygen diffusion during the initial wetting stage. The surface oxides for Kovar(P) and Kovar(L) consist mainly of FeO and Fe<sub>3</sub>O<sub>4</sub>. Contact angle measurements reveal that the wettability characteristics of the Kovar(L) was enhanced. For instance, the contact angle for the Kovar (L) is 38 deg and that for Kovar (P) is 47.5 deg when both holding for 100 min.

The surface oxide scale for both cases has two oxide scales. For Kovar (L) these two oxide scale layers are tightly compacted, while for Kovar (P), there exists a gap between the surface oxide scale and the internal oxide scale. The surface oxygen in the Kovar and the refined grain size resulting from the laser treatment was identified to further assist wetting. The adhesion between the glass and Kovar (L) at both the central region and the fringe region of the interface is very good without cracks, pores, and interfacial delaminations; while for Kovar (P), there exists visible interfacial delaminations in the central region of the interface and pores in the fringe region of the interface. The wustite (FeO) acts as an interlayer in both wetting processes. But no Ni or Co oxides are observed at the glass/Kovar interface and Fe<sub>2</sub>SiO<sub>4</sub> is formed in the mixed region.

This work demonstrates that it is possible to alter the wetting characteristics of Kovar alloy by using a laser to melt the Kovar surface in atmosphere to substitute for the thermal treatment of Kovar under a high temperature to form an oxide scale on the surface. The findings of the work show that with the use of the laser radiation Kovar can achieve the same or better wetting characteristics when compared to the Kovar(P) in the same wetting procedure.

## Acknowledgment

Thanks are extended to Ph.D. candidate, Jenny Ardelean (Advanced Manufacturing Laboratory, Columbia University) for her important assistance in conducting the SEM/EDX tests.

## Funding Data

- National Natural Science Foundation of China (Grant No. 51172221).
- Suzhou Science and Technology Bureau (Grant No. SYG201419).

## References

- [1] do Nascimento, R. M., Martinelli, A. E., and Buschinelli, A. J. A., 2003, "Recent Advances in Metal-Ceramic Brazing," *Ceramica*, **49**(312), pp. 178–198.
- [2] Panjawan, K., Grant, B., and Yao, Y. L., 2015, "Laser Induced Porosity and Crystallinity Modification of a Bioactive Glass Coating on Titanium Substrates," *ASME J. Manuf. Sci. Eng.*, **137**(3), p. 031004.
- [3] Bian, D. K., Bradley, R. B., Shim, D. J., Marshall, J., and Lawrence Yao, Y. L., 2017, "Interlaminar Toughening of GFRP—Part I: Bonding Improvement Through Diffusion and Precipitation," *ASME J. Manuf. Sci. Eng.*, **139**(7), p. 071010.
- [4] Zhang, M. Y., and Gary, J. C., 2011, "Continuous Mode Laser Coating of Hydroxyapatite/Titanium Nanoparticles on Metallic Implants: Multiphysics Simulation and Experimental Verification," *ASME J. Manuf. Sci. Eng.*, **133**(2), p. 021010.
- [5] Zanchetta, A., Lefort, P., and Gabbay, E., 1995, "Thermal Expansion and Adhesion of Ceramic to Metal Sealings: Case of Porcelain-Kovar Junctions," *J. Eur. Ceram. Soc.*, **15**(3), pp. 233–238.
- [6] Wang, X. L., Ou, D. R., Shang, L., Zhao, Z., and Cheng, M. J., 2016, "Sealing Performance and Chemical Compatibility of SrO–La<sub>2</sub>O<sub>3</sub>–Al<sub>2</sub>O<sub>3</sub>–SiO<sub>2</sub> Glasses With Bare and Coated Ferritic Alloy," *Ceram. Int.*, **42**(12), pp. 14168–14174.
- [7] Leone, P., Lanzini, A., Delhomme, B., Villalba, G. A., Santarelli, M., Smeacetto, F., Salvo, M., and Ferraris, M., 2011, "Experimental Evaluation of Planar SOFC Single Unit Cell With Crofer22APU Plate Assembly," *ASME J. Fuel Cell Sci. Technol.*, **8**(3), p. 031009.
- [8] Zanchetta, A., Lortholary, P., and Lefort, P., 1995, "Ceramic to Metal Sealings: Interfacial Reactions Mechanism in a Porcelain-Kovar Junction," *J. Alloys Compd.*, **228**(1), pp. 86–95.
- [9] Peng, L., Zhu, Q. S., Xie, Z. H., and Wang, P., 2016, "Interface Reactions Between Sealing Glass and Metal Interconnect Under Static and Dynamic Heat Treatment Conditions," *ASME J. Electrochem. Energy Convers. Storage*, **12**(6), p. 061009.
- [10] Peng, L., Bai, Y., and Zhu, Q. S., 2017, "Thermal Cycle Stability of Sealing Glass for 8YSZ Coated Cr-Containing Metal Interconnect," *ASME J. Electrochem. Energy Convers. Storage*, **13**(4), p. 041002.
- [11] Chen, S. C., and Vafai, K., 1992, "An Experimental Investigation of Free Surface Transport, Bifurcation, and Adhesion Phenomena as Related to a Hollow Glass Ampule and a Metallic Conductor," *ASME J. Heat Transfer*, **114**(3), pp. 743–751.
- [12] Thompson, L. M., Maughan, M. R., Rink, K. K., Blackketter, D. M., and Stephens, R. R., 2006, "Thermal Induced Stresses in Bridge-Wire Initiator Glass-to-Metal Seals," *ASME J. Electron. Packag.*, **129**(3), pp. 300–306.
- [13] Howard, P. J., and Szkoda, I., 2012, "Corrosion Resistance of SOFC and SOEC Glass-Ceramic Seal Materials in High Temperature Steam/Hydrogen," *ASME J. Fuel Cell Sci. Technol.*, **9**(4), p. 041009.
- [14] Kim, J. H., Song, R. H., and Shin, D. R., 2009, "Joining of Metallic Cap and Anode-Supported Tubular Solid Oxide Fuel Cell by Induction Brazing Process," *ASME J. Fuel Cell Sci. Technol.*, **6**(3), p. 031012.
- [15] Donald, I. W., 1993, "Review: Preparation, Properties, and Chemistry of Glass and Glass-Ceramic Metal Seals and Coatings," *J. Mater. Sci.*, **28**(11), pp. 2841–2886.
- [16] Mantel, M., 2000, "Effect of Double Oxide Layer on Metal Glass Sealing," *J. Non-Cryst. Solids*, **273**(1–3), pp. 294–301.
- [17] Luo, D. W., and Shen, Z. S., 2009, "Wetting and Spreading Behavior of Borosilicate Glass to Kovar," *J. Alloys Compd.*, **477**(1), pp. 407–413.
- [18] Trindade, V., Krupp, U., Hanjari, B. Z., Yang, S. L., Krupp, U., and Christ, H. J., 2005, "High-Temperature Oxidation of Pure Fe and the Ferritic Steel 2.25Cr1Mo," *Mater. Res.*, **8**(4), pp. 365–369.
- [19] Geng, S. J., Qi, S. J., Zhao, Q. C., Ma, Z. H., Zhu, S. L., and Wang, F. H., 2012, "Effect of Columnar Nano-Grain Structure on the Oxidation Behavior of Low-Cr Fe–Co–Ni Base Alloy in Air at 800 °C," *Mater. Lett.*, **80**(1), pp. 33–36.
- [20] Zhang, J. Q., Peng, X., Young, D. J., and Wang, F. H., 2013, "Nano-Crystalline Coating to Improve Cyclic Oxidation Resistance of 304 Stainless Steel," *Surf. Coat. Technol.*, **217**(25), pp. 162–171.
- [21] Liu, L., Yang, Z. G., Zhang, C., Ueda, M., Kawamura, K., and Maruyama, T., 2015, "Effect of Grain Size on the Oxidation of Fe–13Cr–5Ni Alloy at 973 K in Ar–21 vol%O<sub>2</sub>," *Corros. Sci.*, **91**, pp. 195–202.
- [22] Waugh, D. G., Lawrence, J., and Brown, E. M., 2012, "Osteoblast Cell Response to a CO<sub>2</sub> Laser Modified Polymeric Material," *Opt. Lasers Eng.*, **50**(2), pp. 236–247.
- [23] Waugh, D. G., and Lawrence, J., 2011, "Wettability and Osteoblast Cell Response Modulation Through UV Laser Processing of Nylon 6,6," *Appl. Surf. Sci.*, **257**(21), pp. 8798–8812.
- [24] Kietzig, A. M., Hatzikiriakos, S. G., and Englezos, P., 2009, "Patterned Superhydrophobic Metallic Surfaces," *Langmuir*, **25**(8), pp. 4821–4827.
- [25] Silvennoinen, M., 2010, "Controlling the Hydrophobic Properties of Material Surface Using Femtosecond Ablation," *J. Laser Micro/Nanoeng.*, **5**(1), pp. 97–98.
- [26] Bizi-Bandoki, P., Benayoun, S., Valette, S., Beaugiraud, B., and Audouard, E., 2011, "Modifications of Roughness and Wettability Properties of Metals Induced by Femtosecond Laser Treatment," *Appl. Surf. Sci.*, **257**(12), pp. 5213–5218.
- [27] Kam, D. H., Bhattacharya, S., and Mazumder, J., 2012, "Control of the Wetting Properties of an AISI 316L Stainless Steel Surface by Femtosecond Laser-Induced Surface Modification," *J. Micromech. Microeng.*, **22**(10), p. 105019.
- [28] Lawrence, J., and Li, L., 1999, "Carbon Steel Wettability Characteristics Enhancement for Improved Enamelling Using a 1.2 kW High Power Diode Laser," *Opt. Laser. Eng.*, **32**(4), pp. 353–365.
- [29] Loughridge, F. A., and Wong, W. S., 2013, "Improved Reliability of Soft Glass to Metal Vacuum Tight Seals," Sixth National Symposium Vacuum Technology Transactions, Philadelphia, PA, Oct. 7–9, pp. 283–287.
- [30] Fujii, T., Groot, F. M., and Sawatzky, G. A., 1999, "In Situ XPS Analysis of Various Iron Oxide Films Grown by NO<sub>2</sub>-Assisted Molecular-Beam Epitaxy," *Phys. Rev. B*, **59**(4), pp. 3195–3202.
- [31] Muhler, M., Schlogl, R., and Ertl, G., 1992, "The Nature of the Iron-Based Catalyst for Dehydrogenation of Ethylbenzene to Styrene 2—Surface Chemistry of the Active Phase," *J. Catal.*, **138**(2), pp. 413–444.
- [32] Tripp, H. P., and King, B. W., 1955, "Thermodynamic Data on Oxides at Elevated Temperatures," *J. Am. Ceram. Soc.*, **38**(12), pp. 432–437.
- [33] David, J. Y., 2016, *High Temperature Oxidation and Corrosion of Metals*, 2nd ed., Elsevier, London, pp. 85–144.
- [34] Lawrence, J., and Li, L., 1999, "Wettability Characteristics of an Al<sub>2</sub>O<sub>3</sub>/SiO<sub>2</sub>-Based Ceramic Modified With CO<sub>2</sub>, Nd:YAG, Excimer and High-Power Diode Lasers," *J. Phys. D*, **32**(10), pp. 1075–1082.
- [35] Chern, T. S., and Tsai, H. L., 2007, "Wetting and Sealing of Interface Between 7056 Glass and Kovar Alloy," *Mater. Chem. Phys.*, **104**(2–3), pp. 472–478.